Finite element solutions of laminar flow and heat transfer of air in a staggered and an in-line tube bank

Cha'o-Kuang Chen*, King-Leung Wong* and J. W. Cleaver†

A finite element method is used to solve the full Navier–Stokes and energy equations for the problems of laminar flow and heat transfer characteristics of air around three isothermal heated horizontal cylinders in a staggered tube bank and around four isothermal heated horizontal cylinders in an in line tube bank. The variations of surface shear stress, pressure and Nusselt number are obtained over the entire cylinder surface, including the zone beyond the separation point. The predicted values of total drag, pressure drag and friction drag coefficients, average Nusselt number, and the plots of velocity flow fields and isotherms are also presented.

Keywords: *laminar flow, heat transfer, tube banks, finite element solutions, air flow*

Introduction

The study of flow normal to a bank of tubes continues to attract interest because of the importance of this flow configuration in the design of heat exchangers. Many related engineering applications of the heat transfer and flow characteristics of tubes in staggered or in-line tube banks have been presented. Zhukauskas[1] has studied the heat transfer from tubes in cross flow. Bergelin *et al*[2] have presented their investigation of heat transfer and fluid friction during flow across banks of tubes. Massey[3] has predicted the flow and heat transfer in banks of tubes in cross flow. Bergelin *et al*[4] have investigated three tube arrangements in unbaffled tubular heat exchangers. Launder and Massey[5] have presented their numerical prediction of viscous flow and heat transfer in tube banks. Fujii *et al*[6] have presented a numerical analysis of laminar flow and heat transfer of air in an in-line tube bank. Weaver and Abd-Rabbo[7] have presented a flow visualization study of a square array of tubes in water cross flow. Aiba *et al*[8] have investigated experimentally heat transfer around a tube in a staggered tube bank. Antonopoulos[9] has studied the heat transfer in tube assemblies under conditions of laminar axial, transverse and inclined flow.

In the work described here, the problems of heat transfer and flow characteristics around three cylinders in staggered tube banks and four cylinders in in-line tube banks are solved by a finite element method. The method is based on the solution of the full Navier–Stokes and energy equations. The numerical results are obtained over the entire cylinder surface, including the zone beyond the separation point.

* Department of Mechanical Engineering, National Cheng-Kung University, Tainan, Taiwan 700, Republic of China
† Department of Mechanical Engineering, The University of Liverpool, PO Box 147, Liverpool L69 3BX, UK

Problem statement

Consider three and four isothermal heated horizontal cylinders of radius R_0 and temperature T_w, placed in a uniform free stream of temperature T_∞ and velocity u_∞ in staggered and in-line arrangements, respectively, with spacing L between the cylinder centres. The cylinders are considered to be long enough so that the end effects can be neglected, and accordingly the flow field can be assumed to be two-dimensional. Using Cartesian coordinates with x and y axes, the flow configurations and the calculated flow fields are shown in Figs 1 and 2, respectively.

The temperature difference ΔT $(=T_w-T_\infty)$ is assumed to have a neglegible effect on the fluid properties, and the fluid is incompressible. The dimensionless governing equations can be written as follows.

Continuity equation:

$$\frac{\partial u}{\partial x}+\frac{\partial v}{\partial y}=0 \tag{1}$$

Momentum equations:

$$u\frac{\partial u}{\partial x}+v\frac{\partial u}{\partial y}=-\frac{\partial p}{\partial x}+\frac{1}{Re}\left(\frac{\partial^2 u}{\partial x^2}+\frac{\partial^2 u}{\partial y^2}\right) \tag{2}$$

$$u\frac{\partial v}{\partial x}+v\frac{\partial v}{\partial y}=-\frac{\partial p}{\partial y}+\frac{1}{Re}\left(\frac{\partial^2 v}{\partial x^2}+\frac{\partial^2 v}{\partial y^2}\right) \tag{3}$$

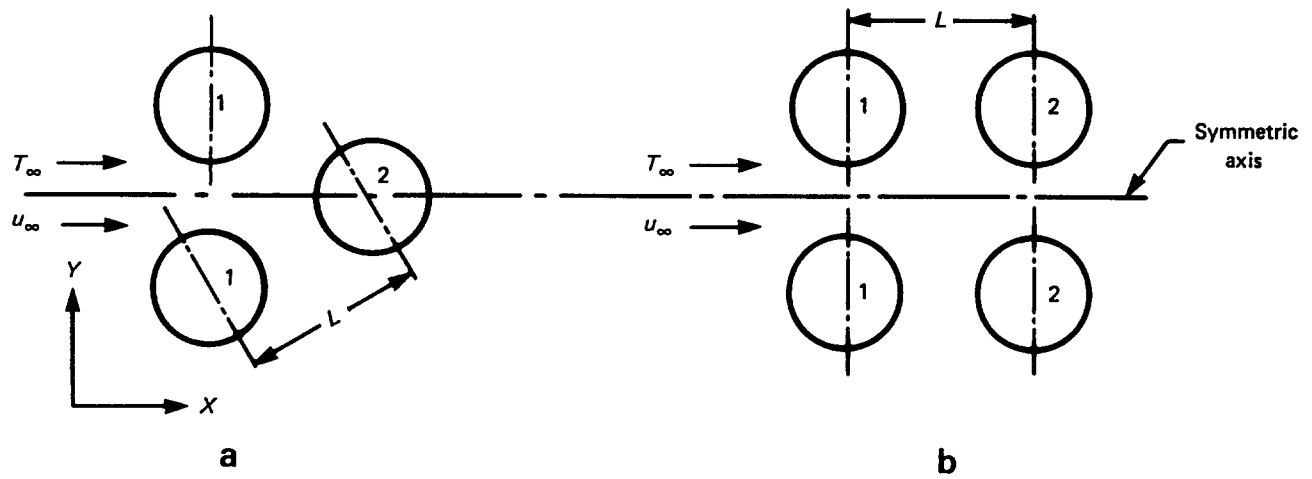

Fig 1 Flow configurations and coordinates: (a) three cylinders; (b) four cylinders

Energy equation:

$$u\frac{\partial\phi}{\partial x}+v\frac{\partial\phi}{\partial y}=\frac{1}{Pe}\left(\frac{\partial^2\phi}{\partial x^2}+\frac{\partial^2\phi}{\partial y^2}\right) \tag{4}$$

where

$$u=\frac{u^*}{u_\infty} \quad v=\frac{v^*}{u_\infty} \quad \phi=\frac{T-T_\infty}{T_w-T_\infty} \quad p=\frac{p^*}{\rho u_\infty^2}$$

$$x=\frac{x^*}{D} \quad y=\frac{y^*}{D} \quad Re=\frac{u_\infty D}{\nu} \quad Pr=\frac{\mu c}{k} \quad Pe=Pr\,Re$$

Finite element solution

Owing to symmetry of the flow field, only one half of the total domain of the flow field need be considered. The calculated flow domains are discretized into 642 elements for the three-cylinder case and 725 elements for the four-cylinder case as shown in Figs 3(a) and 3(b), respectively. All the elements are isoparametric quadrilateral, containing 8 nodes, one at each corner and one at the midpoint of each side of the element. All eight nodes are associated with velocities, and only corner nodes with pressure. Following an accepted practice mentioned by Taylor and Hughes[10] the variation in pressure is depicted by shape functions M_l of one order lower than those, N_j, for defining the velocities and temperature:

$$u=\sum_{j=1}^{8}N_j u_j \qquad v=\sum_{j=1}^{8}N_j v_j$$

$$\phi=\sum_{j=1}^{8}N_j\phi_j \qquad p=\sum_{l=1}^{4}M_l p_l \tag{5}$$

After employing the Galerkin weighted residual approach, Eqs (1–4) take the form of non-linear assembled integral matrix equations. There is a standard procedure

Notation

C	Specific heat
C_D	Total drag coefficient
C_f	Friction drag coefficient
C_p	Pressure drag coefficient
D	Diameter of cylinder
h	Local heat transfer coefficient
K	Thermal conductivity
L	Spacing between centres of cylinders
M_l	Shape function
N_i	Shape function
Nu, $\overline{Nu}$	Local and average Nusselt numbers, respectively
P	Dimensionless pressure $\equiv P^*/\rho u_\infty^2$
P^*, p_∞	Pressure and free stream pressure, respectively
Pe	Peclet number $\equiv Re\,Pr$
Pr	Prandtl number $\equiv \mu c/K$
Re	Reynolds number $\equiv Du_\infty/\nu$
R_0	Radius of cylinder
T	Temperature
T_w	Temperature on cylinder surface (fixed value)
T_∞	Free stream temperature
u	Dimensionless x-direction component of velocity $\equiv u^*/u_\infty$
u^*	x-direction component of velocity
u_∞	Free stream velocity
v	Dimensionless Y-direction component of velocity $\equiv v^*/u_\infty$
v^*	Y-direction component of velocity
X	x-direction axis
x	Dimensionless x-direction coordinate $\equiv x^*/D$
x^*	x-direction coordinate
Y	Y-direction axis
y	Dimensionless Y-direction coordinate $\equiv y^*/D$
y^*	Y-direction coordinate
β	Coefficient of volumetric thermal expansion
θ	Plane angle
μ	Dynamic viscosity
ν	Kinematic viscosity $\equiv \mu/\rho$
ρ	Density of fluid
τ_w	Dimensionless surface shear stress, $\tau_w^*/\rho u_\infty^2$
τ_w^*	Surface shear stress
ϕ	Dimensionless temperature $\equiv T-T_\infty/T_w-T_\infty$

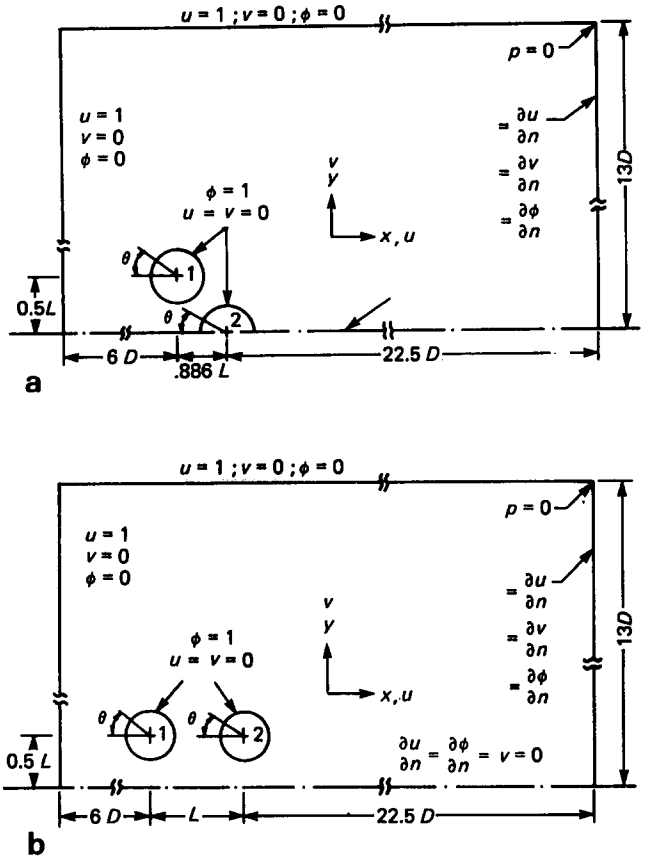

Fig 2 The calculated flow domain, boundary conditions and coordinates of the flow field: (a) three cylinders; (b) four cylinders

in evaluating the above integrations, which is mentioned by Taylor and Hughes[10]. This involves: (i) the normalization of the coordinates, and (ii) the use of the Gauss–Legendre quadrature scheme. In the present work, the 3×3 and 3×1 Gaussian integration sampling point schemes are used for the surface and line integrals, respectively. The resultant non-linear asymmetric matrix equations are solved by a frontal width method and a Newton–Raphson iterative process.

Accuracy and convergency

The calculated flow domain is discretized into 73 8-node element to solve the problem of combined convection from a heated horizontal circular cylinder for $Re = 20$ as well as $Gr = 0$ and 1600. The comparisons of the results with those of Badr[11] are satisfactory (the differences of average Nusselt number being within 1 %). In the present work, a few discretized element numbers were used to find one suitable to obtain a convergent result. It was found that 642 elements for the three-cylinder case and 725 elements for the four-cylinder case could provide a very good convergent numerical result. The numerical work was done on a CDC Cyber 172 computer. The minimum CPU time was 785 s, and the maximum CPU time was 2344 s.

Physical parameters

(*i*) *Shear stress*

The shear stress is defined as

$$\tau_w^* = \mu \frac{\partial u_t^*}{\partial n^*} = \frac{\mu u_\infty}{D} \frac{\partial u_t}{\partial n} \tag{6}$$

where $\partial u_t / \partial n$ denotes the dimensionless derivative of velocity tangential to the normal direction at the cylinder surface.

The dimensionless shear stress is defined as

$$\tau_w = \frac{\tau_w^*}{\frac{\rho u_\infty^2}{2}} = \frac{u}{\rho u_\infty D} \frac{\partial u_t}{\partial n} = \frac{1}{Re} \frac{\partial u_t}{\partial n} \tag{7}$$

(*ii*) *Friction drag coefficient*

The friction drag coefficient is defined as

$$C_f = \int_0^{2\pi} \frac{2\tau_w}{D} \sin\theta \, r \, d\theta \tag{8}$$

(*ii*) *Pressure drag coefficient*

The total pressure drag force is

$$F_p = \int_0^{2\pi} P^* \cos\theta \, r \, d\theta \tag{9}$$

The pressure drag coefficient is defined as

$$C_p = \frac{F_p}{\frac{1}{2} \rho u_\infty^2 D} \tag{10}$$

(*iv*) *Total drag coefficient*

The total drag coefficient is the summation of friction drag and pressure drag coefficients:

$$C_D = C_f + C_p \tag{11}$$

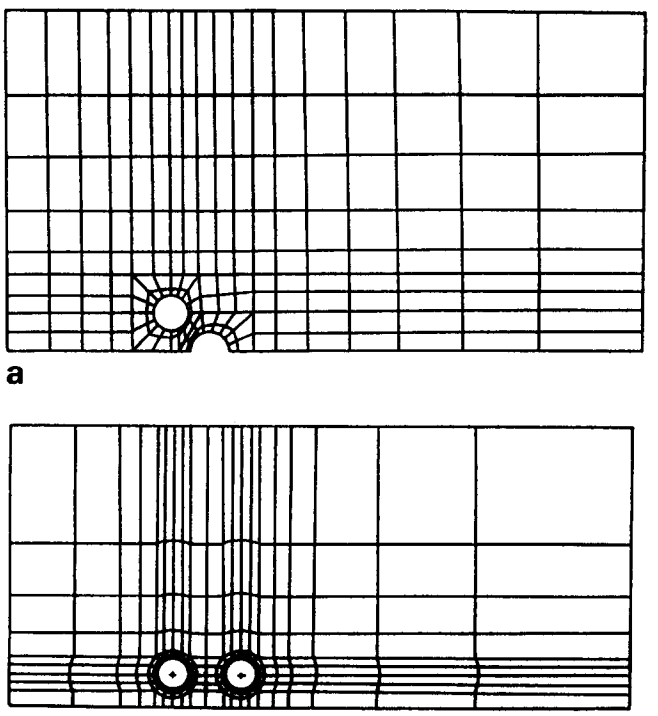

Fig 3 Element discretization of the calculated flow domain: (a) three-cylinder case; (b) four-cylinder case

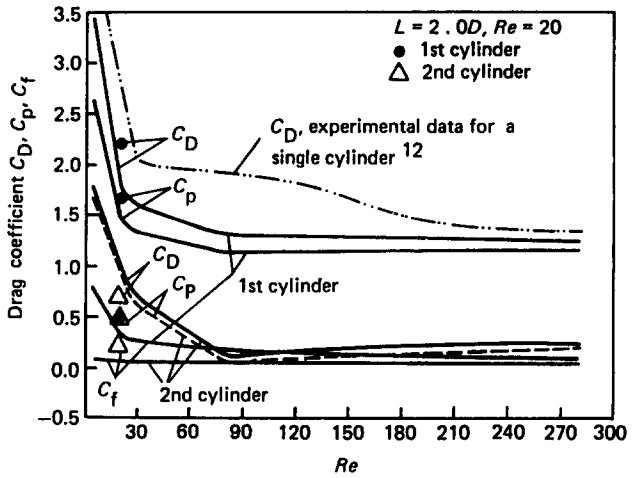

Fig 4 Total drag, pressure drag and friction drag coefficients, C_D, C_p and C_f, for the three-cylinder case (L=1.25D)

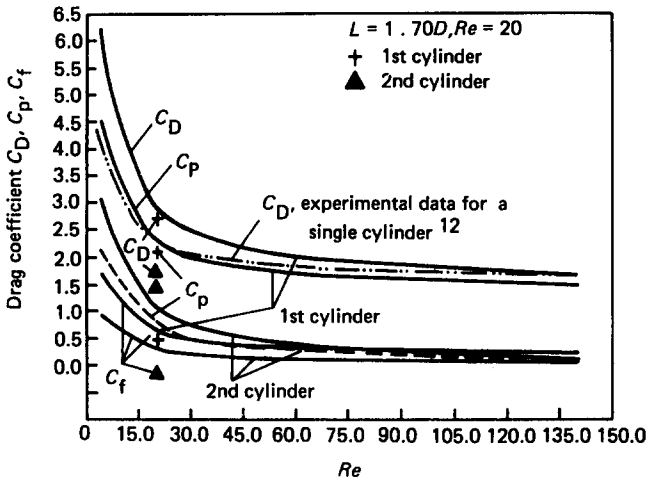

Fig 5 Total drag, pressure drag and friction drag coefficients, C_D, C_p and C_f, for the four-cylinder case (L=2.0D)

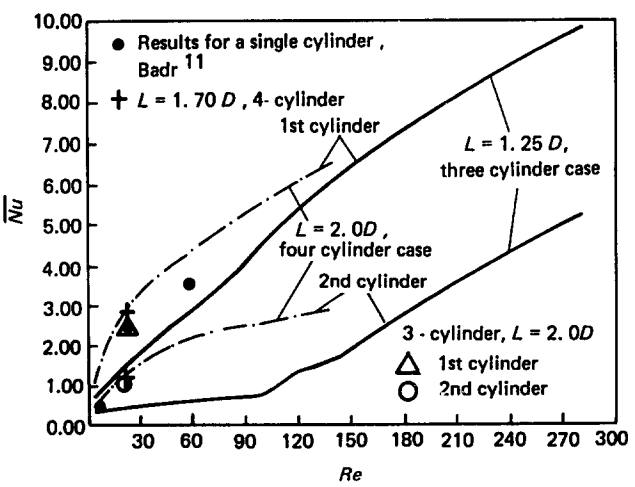

Fig 6 Average Nusselt number $\overline{\text{Nu}}$ *versus Reynolds number* Re

(v) *Nusselt number*

Since the conductive heat transfer rate of the fluid over the solid boundary equals its convective heat transfer rate,

$$-K\nabla^* T = h(T_w - T_\infty) \quad \text{or} \quad -K\frac{1}{D}\nabla\phi = h$$

and the local Nusselt number is

$$Nu = \frac{hD}{k} = -\nabla\phi = -\frac{\partial N_j}{\partial n}\phi_j \tag{12}$$

where $j=1,2,\ldots,8$. The average Nusselt number is defined as

$$\overline{Nu} = \frac{1}{2\pi}\int_0^{2\pi} Nu\, d\theta \tag{13}$$

Results and discussions

The variations of total drag, pressure drag and friction drag coefficients with *Re* for the three-cylinder and four-cylinder cases are shown in Figs 4 and 5, respectively. And the variations of average Nusselt number with *Re* for the three-cylinder and four-cylinder cases are shown in Fig 6. It can be seen from Figs 4 to 6 that for the case of $Re=20$, the greater the value of L the greater will be the values of $\overline{Nu}$, C_f, C_p and C_D for the 1st cylinder. For the 2nd cylinder, the greater the value of L the greater will be the values of the $\overline{Nu}$ and C_f but the smaller will be those of C_p and C_D. It can also be seen that the greater the value of *Re* the greater will be $\overline{Nu}$ but the smaller will be C_f, C_p and C_D except for the values of C_p and C_D for the 2nd cylinder of the three-cylinder case when $Re>80$. It is shown that the experimental data on C_D from Ref 12, and the previous numerical results of $\overline{Nu}$ presented by Badr[11], are close to those for the 1st cylinder, especially for the case of high *Re* or *L*.

The dimensionless surface shear stress distributions for the three-cylinder and four-cylinder cases are shown in Figs 7 and 8, respectively. It is clear from Fig 7 that for the three-cylinder case, increase in *Re* causes a significant decrease in the upper region of the 1st cylinder from 0° to 135° and causes a quite complicated variation in the other region of the 1st cylinder and the entire region of the 2nd cylinder. From Fig 5 it can be seen that for the situation of $L=1.25D$ the C_f value for the 1st cylinder decreases as *Re* increases, and the C_f value for the 2nd cylinder remains almost constant. In Fig 8 it is shown that the variations of surface shear stress for the 1st and 2nd cylinders of the four-cylinder case with $L=2.0D$ are similar; increase in *Re* results in a significant decrease in τ_w for most of the region except near the lower front ($\theta=360°$) and rear stagnation ($\theta=180°$) points. For both the three-cylinder and four-cylinder cases in Figs 7 and 8, the greater the value of *Re* the closer will be τ_w. Thus, it is shown in Figs 4 and 5 that the greater the value of *Re* the closer will be C_f. It can be seen from Eq (7) that $Re\,\tau_w = \partial u_t/\partial n$. Where $Re\,\tau_w \leqslant 0$ separation flow occurs. It is also clear from Figs 7 and 8 that increase in *Re* tends to create an earlier separation flow near the rear stagnation points ($\theta=180°$) of the 1st and 2nd cylinders (Badr[11] predicted the same phenomenon for the situation of a single cylinder) but the effects of the increase in *Re* on the shift of the separation flow near the upper and lower front stagnation points ($\theta=0°$ and $\theta=360°$) are complicated.

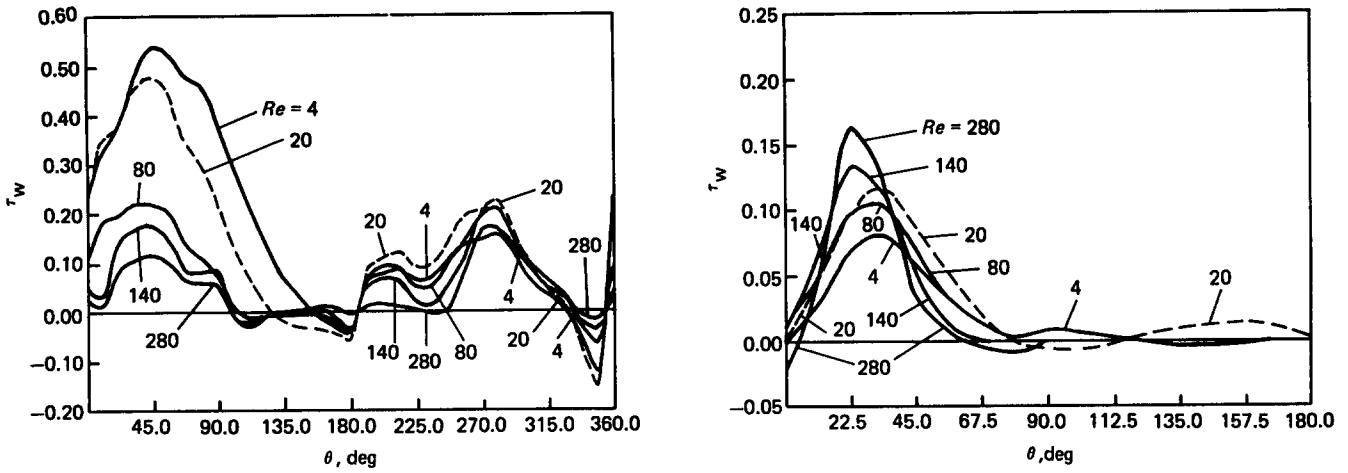

Fig 7 Surface shear stress distribution at PR = *0.7 for the three-cylinder case* (L = *1.25*D): (*a*) *upstream cylinder;* (*b*) *down stream cylinder*

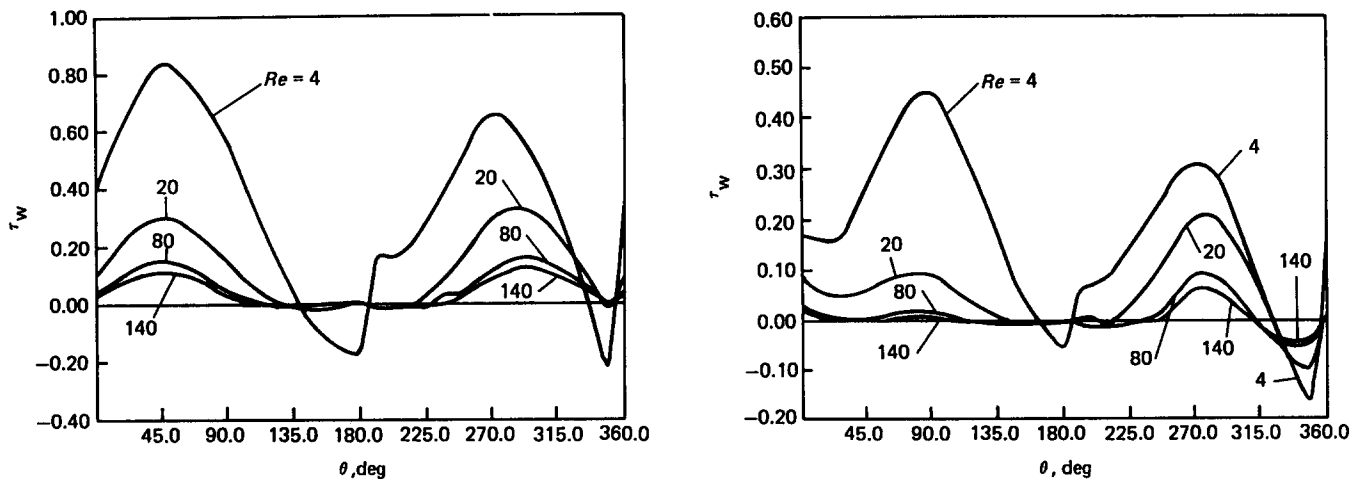

Fig 8 Surface shear stress distribution at Pr = *0.7 for the four-cylinder case* (L = *2.0D*): (*a*) *upstream cylinder;* (*b*) *downstream cylinder*

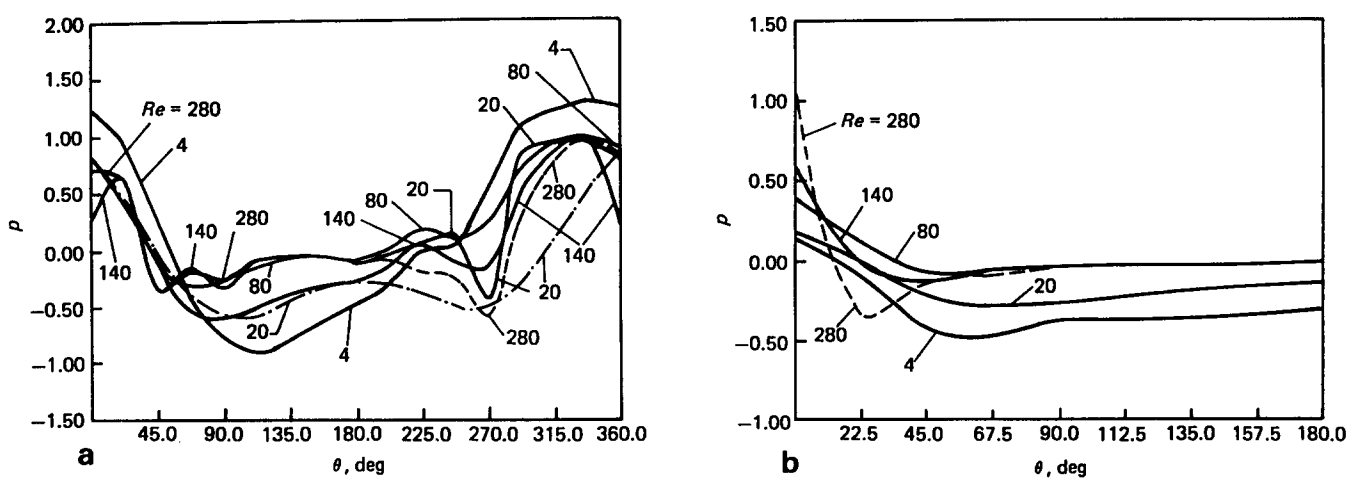

Fig 9 Surface pressure distribution at Pr = *0.7 for the three-cylinder case* (L = *1.25*D): (*a*) *upstream cylinder;* (*b*) *downstream cylinder*

The dimensionless surface pressure distributions for the three-cylinder and four-cylinder cases, with a comparison with the previous result for a single cylinder obtained by Dennis and Chang[13], are given in Figs 9 and 10, respectively. It can be seen from Fig 9 that increase in *Re* tends to create a quite complicated variation for the case of three cylinders with $L = 1.25D$. It can be seen from Fig 4 that for the 1st cylinder C_p decreases as *Re* increases. For the 2nd cylinder when $Re < 80$ C_p decreases as *Re* increases; when $Re > 80$, C_p increases as *Re* increases. It can be seen from Fig 10 that when $Re > 20$ the shapes of the pressure distributions are similar to each other;

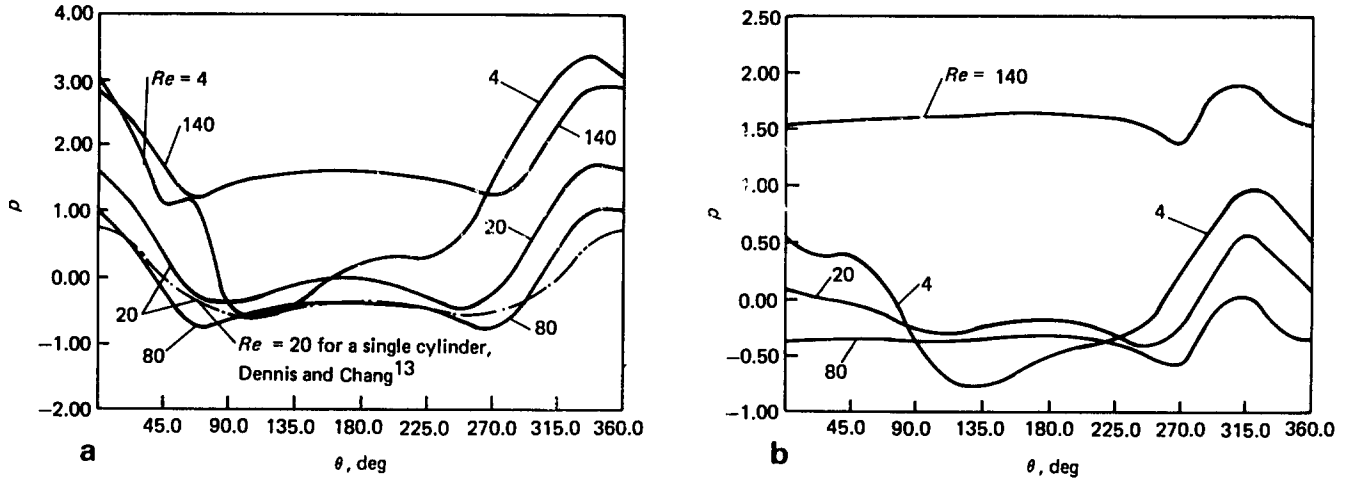

Fig 10 Surface pressure distribution at Pr = *0.7 for the four-cylinder case* (L = *2.0*D): (*a*) *upstream cylinder*; (*b*) *downstream cylinder*

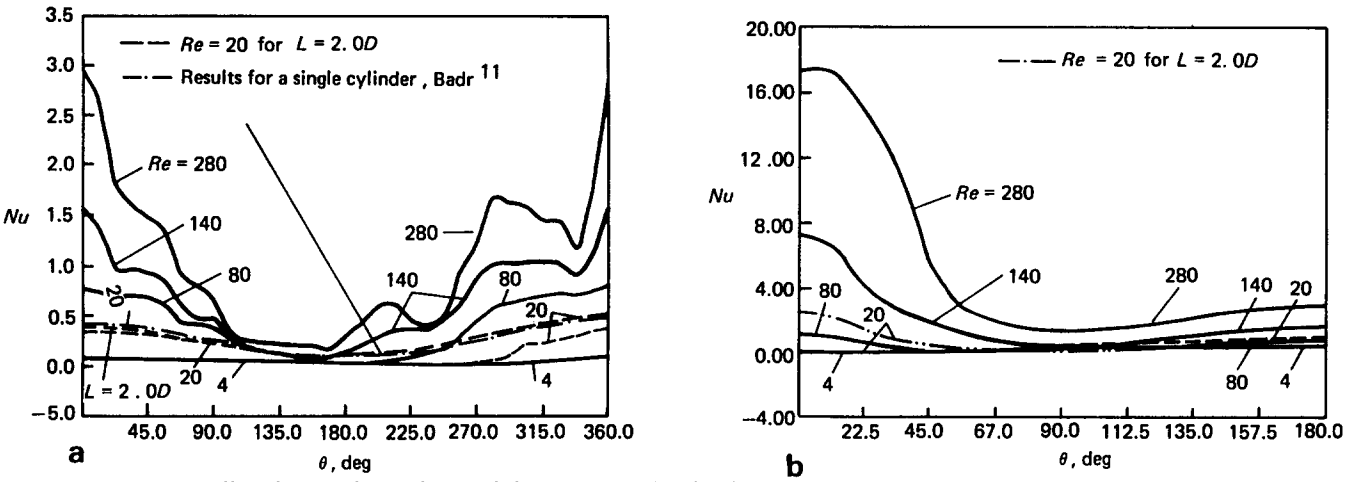

Fig 11 Variation of local Nusselt number with θ *at* Pr = *0.7 for the three-cylinder case* (L = *1.25*D): (*a*) *upstream cylinder*; (*b*) *downstream cylinder*

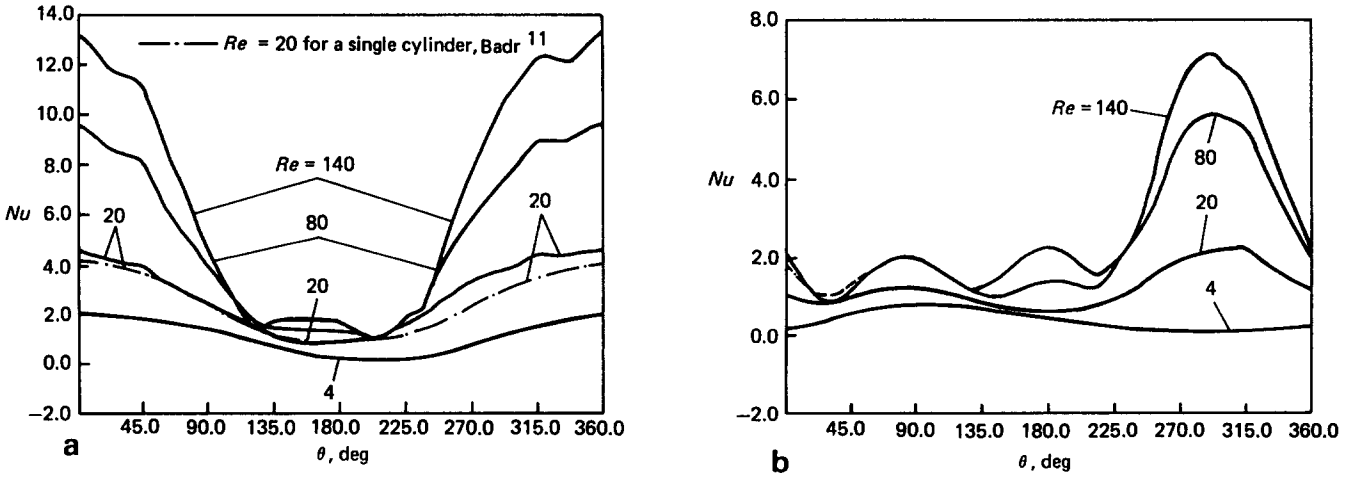

Fig 12 Variation of local Nusselt number with θ *at* Pr = *0.7 for the four-cylinder case* (L = *2.0*D): (*a*) *upstream cylinder*; (*b*) *downstream cylinder*

accordingly a close value of C_p results in Fig 4 for high *Re*. It is also shown in Figs 9(a) and 10(a) that the variation in *P* of a single cylinder (after Dennis and Chang[13]) is close to that of the 1st cylinder, especially in the upper region (0°–180°).

The local Nusselt number distribution for the three-cylinder and four-cylinder cases, with a comparison with the results for a single cylinder obtained by Badr[11], are given in Figs 11 and 12, respectively. It is clear from Figs 11 and 12 that increase in *Re* results in a significant increase in *Nu* for most regions of the cylinders. The variations in *Nu* of the 1st cylinder for both the three-

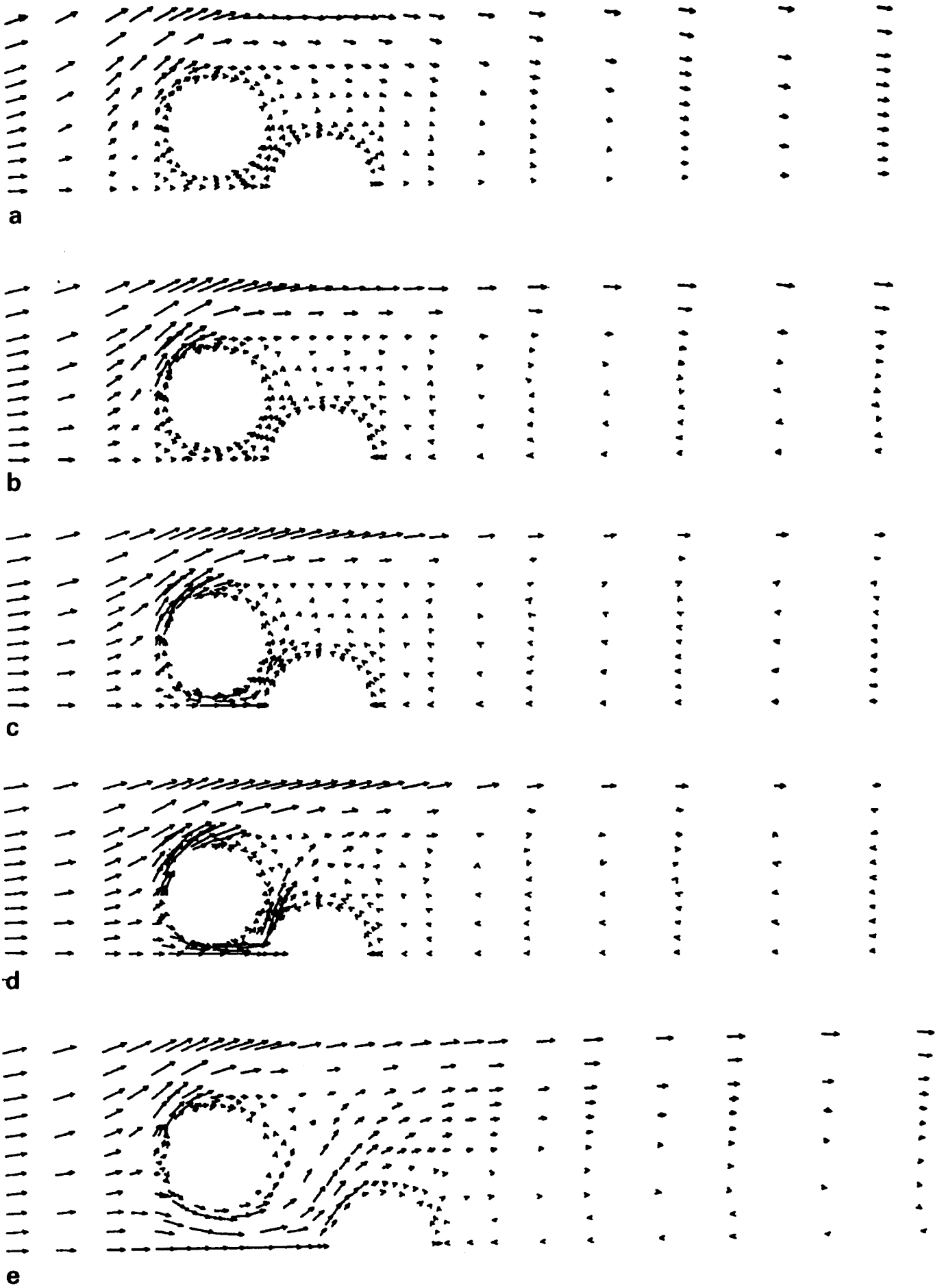

Fig 13 Velocity flow field for three-cylinder case: (*a*) L = *1.25*D, Re = *4*; (*b*) L = *1.25*D, Re = *20*; (*c*) L = *1.25*D, Re = *80*; (*d*) L = *1.25*D, Re = *280*; (*e*) L = *2.0*D, Re = *20*

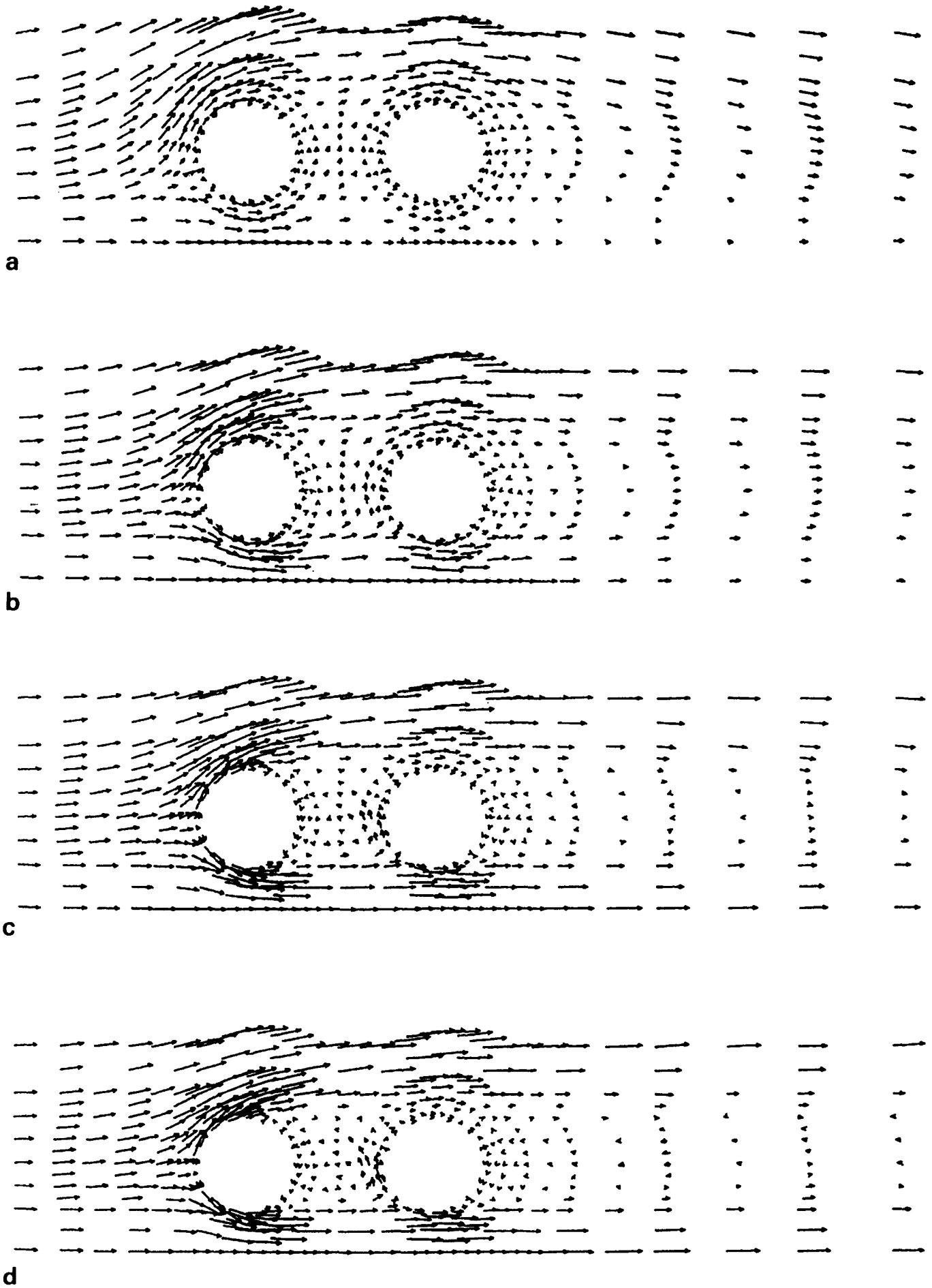

Fig 14 Velocity flow field for four-cylinder case (L = *2.0*D): (*a*) Re = *4*; (*b*) Re = *20*; (*c*) Re = *80*; (*d*) Re = *140*

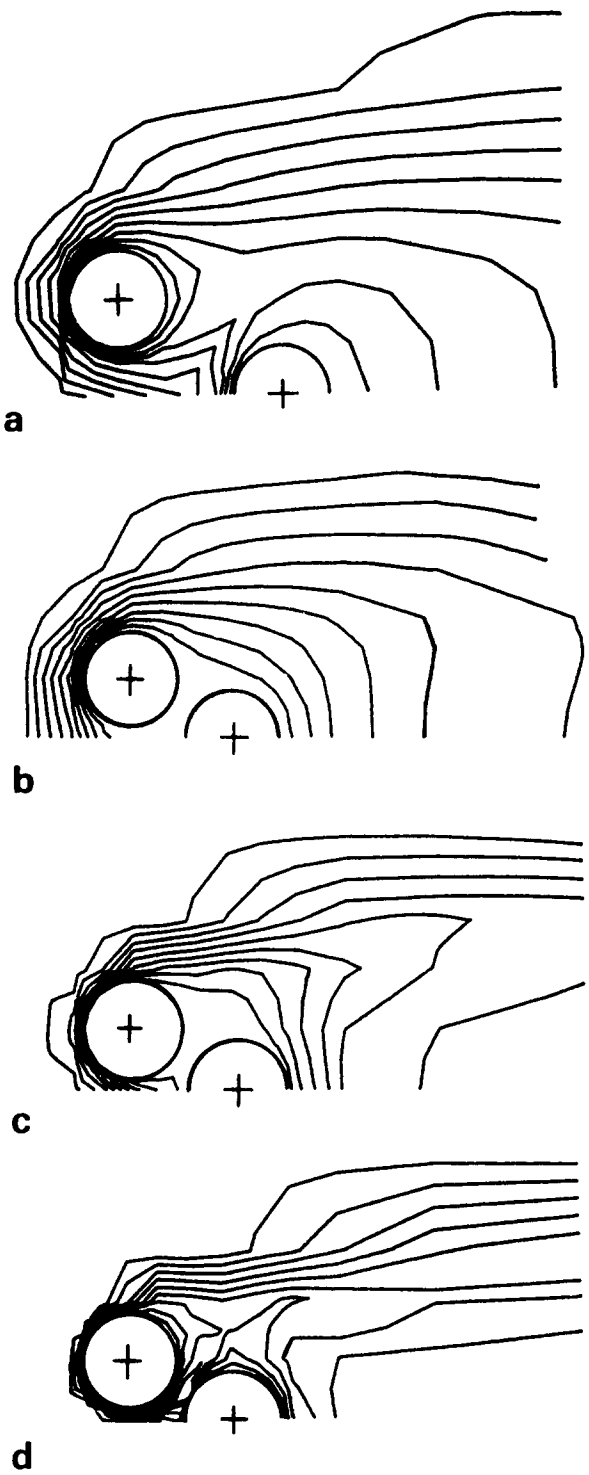

Fig 15 Isotherms for three-cylinder case (the isotherms are 1.0 to 0.1 in decrements of 0.1): (a) L = *2.0*D, Re = *20*; *(b)* L = *1.25*D, Re = *20*; *(c)* L = *1.25*D, Re = *80*; *(d)* L = *1.25*D, Re = *140*

cylinder and four-cylinder cases are similar. The maximum *Nu* occurs at the front stagnation point ($\theta = 0°$ or $\theta = 360°$) and the minimum *Nu* occurs at the rear stagnation point ($\theta = 180°$). But the variations in *Nu* of the 2nd cylinders are quite different; *Nu* is relatively high in the front region (0°–45°) for the 2nd cylinder of the three-cylinder case, and is relatively small in the upper region (0°–180°) for the 2nd cylinder of the four-cylinder case. It can also be seen from Figs 11(a) and 12(a) that the result for a single cylinder obtained by Badr[11] is close to that for the 1st cylinder, especially for the upper region (0°–180°).

The velocity flow fields for the three-cylinder and four-cylinder cases are shown in Figs 13 and 14, respectively. The isotherms for the three-cylinder and four-cylinder cases are shown in Figs 15 and 16,

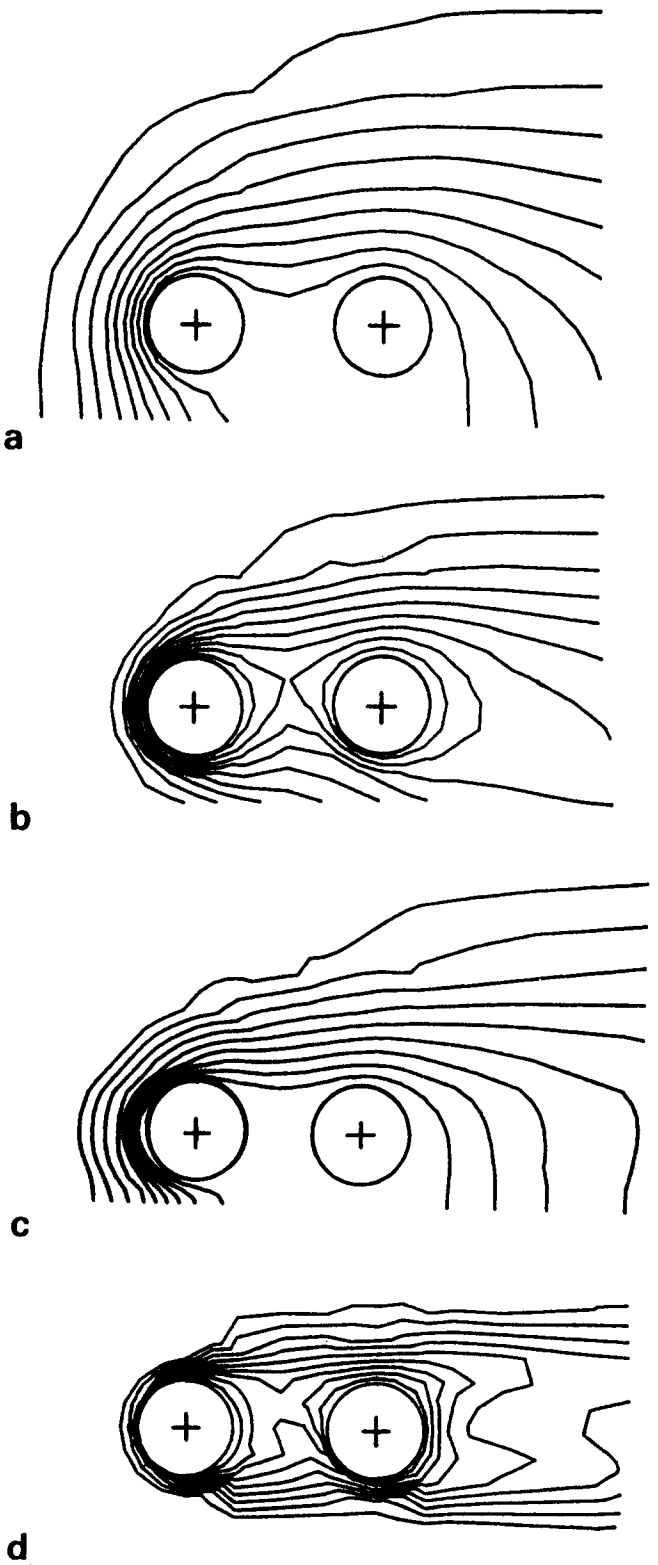

Fig 16 Isotherms for four-cylinder case (isotherms as in Fig 15): (a) Re = *4*, L = *2.0*D; *(c)* Re = *20*, L = *1.70*D; *(d)* Re = *140*, L = *2.0*D

respectively. It is clear from Figs 13(b) and 13(e) that for the same Re ($Re=20$), the greater the value of L the greater will be the velocity in the lower region (180°–360°) of the 1st cylinder and the region between the 1st and 2nd cylinders for the three-cylinder case. The heat transfer rate depends on both temperature difference ($T_w - T$) and velocity. It can be seen from Fig 15(b) that there exists no isotherm line in the region between the 1st and 2nd cylinders for $Re=20$ and $L=1.25D$, but not for the case of $Re=20$ and $L=2.0D$ shown in Fig 15(a). This phenomenon may be interpreted as follows: when L is too small, the flow in the lower region of the 1st cylinder is blocked by the 2nd cylinder as well as the narrow path between the 1st and 2nd cylinders; accordingly a smaller velocity and a lower heat transfer rate result. It can also be seen from Fig 16(c) that for the situation of $Re=20$ and $L=1.70D$ there exists no isotherm line in the region between the 1st and 2nd cylinders (accordingly a lower heat transfer rate results), but not for the case of $Re=20$ and $L=2.0D$ shown in Fig 16(b). For fixed values of diameter D and viscosity ν, the effect of increase in Re is to increase velocity. From Figs 15 and 16 it can be seen that as Re increases, the isotherm lines move closer to the cylinder surface. For the dense isotherm regions, where heat transfer rate is high, there exists either a greater $T_w - T$ (such as at $\theta=0°$ for the 1st cylinder) or a greater velocity (such as the lower region near $\theta=270°$ for the 1st cylinder, the path between the 1st and 2nd cylinders for the three-cylinder case with $L=2.0D$, and the regions near $\theta=90°$ and 270° for the four-cylinder case). Increase in Re results in earlier separation flow. Accordingly, it can be seen from Figs 4 and 5 that the greater the value of Re the smaller will be C_f. For the 1st cylinder of the three-cylinder case with $L=2.0D$, and the 1st and 2nd cylinders of the four-cylinder case, the velocity in the lower region from 270° to 315° is greater than that in the upper region from 45° to 90°. This phenomenon may be caused by the nozzle effect. Thus, that heat transfer rate of the region from 270° to 315° is greater than that of the region from 45° to 90° for the above cases shown in Figs 11 and 12 as well as Figs 15 and 16.

Conclusions

The finite element solutions of laminar flow and heat transfer of air from three cylinders in a staggered arrangement and from four cylinders in an in-line arrangement were obtained on the basis of the full Navier–Stokes and energy equations. The numerical results were obtained over the entire surface of the cylinder, including the zone beyond the separation point. It was found that the effects of the parameter Re on the variations of the total drag, friction drag and pressure drag, the increase of heat transfer rate, and the shift of the location of separation flow are significant. From comparison with previous results for a single cylinder it was found that the behaviour of the upper region of the upstream cylinder is close to that of a single cylinder. The greater the spacing between the cylinders the closer are the present results to those for a single cylinder.

References

1. **Zhukauskas A.** Heat transfer from tubes in cross flow. *Advances in Heat Transfer, 1972*, **8**, *93–160*
2. **Bergelin O.P., Brown G. A. and Doberstein S. C.** Heat transfer and fluid friction during flow across banks of tubes—IV. *Trans. ASME, 1952*, **74**, *953–960*
3. **Massey T. H.** The prediction of flow and heat transfer in banks of tubes in cross-flow. *PhD thesis, Central Electricity Research Laboratories, Leatherhead, Surrey, February 1976*
4. **Bergelin O. P., Davis E. S. and Hull H. L.** A study of three tube arrangements in unbaffled tubular heat exchangers. *Trans. ASME, 1949*, **71**, *369–374*
5. **Launder B. E. and Massey T. H.** The numerical prediction of viscous flow and heat transfer in tube banks. *Trans. ASME, J. Heat Transfer, Nov 1978*, **100**, *565–571*
6. **Fujii M., Fujii T. and Nagata T.** A numerical analysis of laminar flow and heat transfer of air in an in-line tube bank. *Numerical Heat Transfer, 1984*, **7**, *89–102*
7. **Weaver D. S. and Abd-Rabbo A.** A flow visualization study of a square array of tubes in water crossflow. *Trans. ASME, J. Fluids Eng., Sept 1985*, **107**, *354–363*
8. **Aiba S., Tsuchida H. and Ota T.** Heat transfer around a tube in a staggered tube bank. *Trans. JSME, 1982*, **48**, *1976–1984*
9. **Antonopoulos K. A.** Heat transfer in tube assemblies under conditions of laminar axial, transverse and inclined flow. *Int. J. Heat and Fluid Flow, Sept 1985*, **6**(*3*), *193–204*
10. **Taylor C. and Hughes T. G.** *Finite Element Programming of the Navier–Stokes Equations, Pineridge Press, Swansea, 1981, 30–119*
11. **Badr H. H.** Laminar combined convection from a horizontal cylinder—parallel and contra flow regimes. *Int. J. Heat Mass Transfer, 1984*, **27**(*1*), *15–27*
12. **Fox R. W. and McDonald A. T.** *Introduction to Fluid Mechanics, third edn, The Southeast Book Company, John Wiley and Sons, New York, 1985, 463*
13. **Dennis S. C. R. and Chang G.** Numerical solutions for steady flow past a circular cylinder at Reynolds numbers up to 100. *J. Fluid Mech., 1970*, **42**, *471–489*

Books received

Lecture Notes in Engineering, *ed C. A. Brebbia and S. A. Orszag*, Vol 18

Numerical simulation of fluid flow and heat/mass transfer processes, *eds N. C. Markatos, D. G. Tatchell, M. Cross and N. Rhodes*, DM72 pp 482, Springer Verlag